ACS APPLIED MATERIALS & INTERFACES

Research Article

www.acsami.org

Creation of Reduced Graphene Oxide Based Field Effect Transistors and Their Utilization in the Detection and Discrimination of Nucleoside Triphosphates

Chunmeng Yu,[†] Xingmao Chang,[‡] Jing Liu,[†] Liping Ding,[†] Junxia Peng,[†] and Yu Fang*[,†]

[†]Key Laboratory of Applied Surface and Colloid Chemistry of Ministry of Education, School of Chemistry and Chemical Engineering, Shaanxi Normal University, Xi'an 710119, People's Republic of China

[‡]Key Laboratory of Applied Surface and Colloid Chemistry of Ministry of Education, School of Materials Science and Engineering, Shaanxi Normal University, Xi'an 710119, People's Republic of China

Supporting Information

ABSTRACT: Two low-cost, micropatterned, solution-gated field effect transistors (modified FET and unmodified FET) based on reduced graphene oxide (RGO) were developed and used for detection and discrimination of nucleoside triphosphates (NTPs). The modified FET was realized by simple deposition of a positively charged bis-pyrenyl derivative, py-diIM-py, onto the conducting RGO strips of the unmodified FET. The electrical properties and sensing behaviors of the as-prepared devices were studied comprehensively. Electrical transfer property tests revealed that both of the two FETs exhibit V-shaped ambipolar field effect behavior from *p*-type region to *n*-type region. Sensing performance studies demonstrated that modification of the native FET with py-diIM-py improves its sensing ability to NTPs—GTP and ATP in particular. The detection limit of GTP and ATP was as low as 400 nM, which is the lowest value for graphene-based electronic sensors reported so far. Furthermore, based on the cross-reactive responses of the two devices to NTPs, NTPs can be conveniently distinguished via combining use of the two devices. The enhancement of the modifier (py-diIM-py) to the sensing performance of the FET is tentatively attributed to its possible mediation role in sticking onto RGO strips and accumulating analytes by electrostatic association with the relevant species. Because they are sensitive and fast in response, simple and low-cost in preparation, and possibly useful in sensor-array fabrication, the developed sensors show great potential in real-life application.

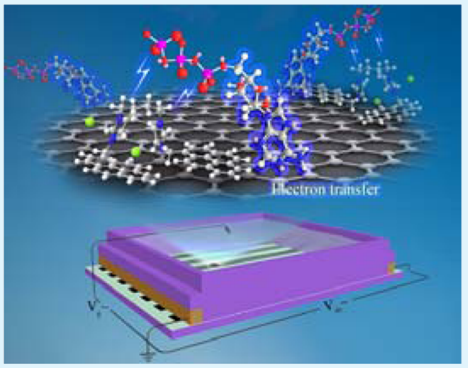

KEYWORDS: *reduced graphene oxide, field-effect transistors, nucleoside triphosphates detection, noncovalent modification, nanoelectronic sensor*

INTRODUCTION

Graphene, the thinnest known material, has attracted increasing attention in both materials science and condensed-matter physics for the past decade. It is a single layer of highly crystalline graphite with a two-dimensional hexagonal honeycomb-like structure and is considered as the basic building block for graphitic materials of every other dimensionality.[1,2] Graphene exhibits superior mechanical strength, fascinating thermal stability, and excellent electrical charge carrier mobility.[3,4] Therefore, graphene has been applied in many fields, such as transparent conducting electrodes,[5,6] solar cells,[7,8] electronic devices,[1,9] supercapacitors,[10] energy storage,[11] and sensors.[12,13] For acute perception to environmental changes,[14] graphene has been employed in fabricating sensors to detect analytes such as gases,[9,15] metal ions,[16,17] bacterials,[18] and biological materials.[12] Graphene-based field effect transistors (GFETs), especially graphene-based solution-gated FET (GSFET) systems, have an advantage of combing the functions of sensor and amplifier.[19,20] In addition, the FETs are cost-effective, space saving, and quite stable when used in liquid phase. These outstanding properties enable GSFETs to be wildly applied in constructing biosensors with excellent sensing performances.[12,21] Most of the GSFETs devices are designed for sensing DNA,[22,23] cell,[18] glucose,[24] and proteins.[25,26] However, studies of FETs for nucleotides sensing are still limited,[27] not to mention discrimination of the structurally similar nucleotides.

Sensitive and selective detection of nucleotide anions is of great importance for their significant role in the wide areas of biology, chemical processes, and environmental sciences. It has attracted great interest over the last few decades.[28−30] Due to generally providing energy and phosphate group for phosphorylations, nucleoside triphosphates (NTPs) have attracted increasing attentions. NTPs mainly include adenosine-5′-

Received: January 7, 2015
Accepted: May 6, 2015
Published: May 6, 2015

DOI: 10.1021/acsami.5b00155
ACS Appl. Mater. Interfaces 2015, 7, 10718−10726

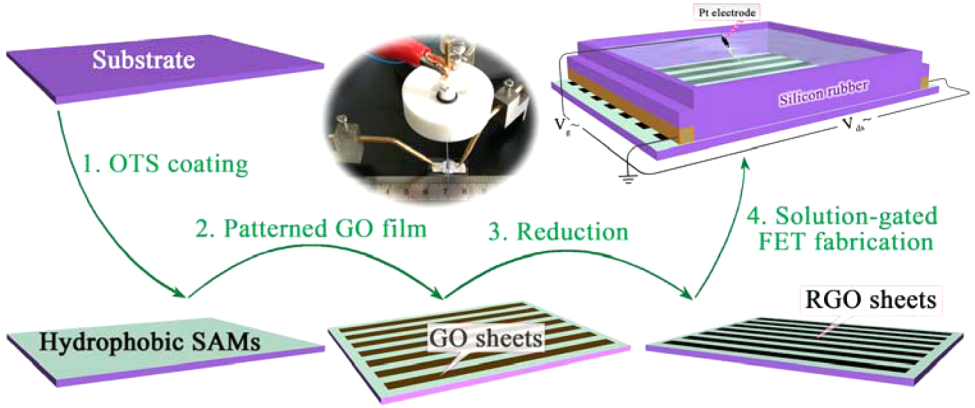

Figure 1. Schematic illustration of fabrication processes of micropatterned RGO solution-gated FET. (1) Hydrophobic OTS SAMs form on the substrate. (2) OTS substrate with micropatterned mask was first exposed to UV light, and then GO suspension was deposited on the hydrophilic area to obtain micropatterned GO film. (3) The patterned GO film was chemically and thermally reduced to obtain the conducting RGO. (4) The RGO substrate is contacted with insulated Ag electrode from two sides and the sensing chamber is defined by silicon rubber. (Inset) Photo of RGO solution-gated FET.

triphosphate (ATP), guanosine-5′-triphosphate (GTP), cytidine-5′-triphosphate (CTP), uridine-5′-triphosphate (UTP), and thymine-5′-triphosphate (TTP). Among the NTP anions, ATP and GTP are more critical since ATP plays an important role in energy transduction in organisms and controls of several metabolic processes, whereas GTP is a nucleotide involved in RNA synthesis as well as the citric acid cycle. In addition, GTP acts as an energy source for protein synthesis. Generally, fluorescent and mass spectrometry methods with high sensitivity and selectivity have been widely used for detection of ATP or GTP.[29,31−34] However, these methods or techniques are subjected to high cost, tedious synthesis steps, complex fabrication process, complicated instruments, or requirement for labeled probes. Moreover, it is still very difficult to discriminate NTPs due to their similarity in chemical structures. Therefore, developing new and label-free detection methods with great sensitivity, high selectivity, fast response, low-cost, and even small size is very urgent.

In the present study, two solution-gated FETs with continuous reduced graphene oxide (RGO) stripes as micropatterned conductive channels were prepared. And the RGO strips on one of the devices were modified by a bis-pyrenyl derivative, py-diIM-py, to improve its performance in NTPs sensing. Furthermore, the sensing performance of the two devices can be also modulated by varying the operating gate voltage. It has been demonstrated that the performance at *p*-type region is superior to that at *n*-type region. Sensing studies revealed that the py-diIM-py modified RGO-based FET sensor possesses fast, selective and sensitive response to GTP and ATP, and the detection limit is as low as 400 nM, the lowest reported result for electronic sensors until now. In addition, based on their cross-reactive responses to the NTPs, discrimination of the five mentioned NTPs could be realized by combing the responses of the two sensors.

EXPERIMENTAL METHODS

Preparation of GO Suspensions. A certain amount of GO (Scheme S1, Supporting Information) was put into a certain amount of water. The mixture was sonicated gently for 20 min, and then it was centrifuged at 1500 rpm for 25 min to remove all thick multilayer flakes. After that, the top layer solution was collected and further centrifuged at 8500 rpm for another 25 min to separate larger GO sheets from the smaller ones. The obtained precipitates were redispersed in water/ethanol (v/v = 1:2) mixture to get a suspension of larger GO sheets for further studies.

Fabrication of Micropatterned RGO-based Solution-Gated FETs. The fabrication process is shown in Figure 1. First, a precleaned glass plate was treated by octadecyltrichlorosilane (OTS) in vacuum at 120 °C for 220 min to obtain an OTS self-assembled monolayers (SAMs) on surface. Then, the substrate was covered by a micropatterned mask (100 μm width, 100 μm gap) and exposed to UV light (homemade UV light equipment, 1000 W) for 90 min. After that, a GO suspension was deposited on the substrate surface via spin-coating at a speed of 1000 rpm for 60 s. The obtained GO film was further treated in hydrazine vapor at 60 °C for 12 h, and then annealed in Ar atmosphere at 200 °C for 2 h to obtain a RGO film with microstrip patterns. Finally, the conductive silver paste as source and drain electrodes were deposited on the patterned RGO films, which was annealed at 80 °C for 60 min in vacuum to enhance the contact between the RGO sheets and electrodes. Silicon rubber was used to encapsulate the source and drain electrodes to minimize leakage current. The silicon rubber insulated the electrodes completely and defined the size of the sensing chamber (3 mm in width, 6 mm in length).

Surface Modification of the FETs with py-diIM-py. The RGO sheets on the conducting channels of the device were put into the methanol solution of py-diIM-py (0.1 μM) at room temperature. The modifier was firmly adsorbed on the RGO strips due to strong $\pi-\pi$ interaction and extra-modifier was removed by washing with deionized (DI) water.

Electrical Measurements. To test the electrical property of the prepared device, 60 μL of DI water was injected into the chamber, and a Pt wire was inserted as an electrode to modulate the gate voltage of the device. The source-drain current (I_{ds}) was continuously recorded at a given source-drain voltage (V_{ds} = 400 mV) and the analyte of various concentrations was added. The gate voltage (V_{gs}) was applied at −0.6, 1.2 V via Pt electrode immersed in the solution.

Instrumentations. All electrical measurements were conducted on an instrument of Agilent B2912A precision source/measure unit and at ambient temperature and pressure. The XRD traces were collected by a Rigalcu D/Max-3c diffractometer with Cu Kα (λ = 0.154 nm) radiation generated at 40 kV and 30 mA as light source. The scan rate was 4°/min. The test sample was prepared by placing a graphite powder or freeze-dried GO directly onto a glass sample holder. The FTIR spectra were obtained with a Bio-Rad FTIR spectrometer, and the attenuated total reflection infrared (ATR-IR) spectra of the films were recorded with a Bruker VERTEX 70v spectrometer. AFM pictures were obtained using Veeco Dimension V (noncontact mode). Contact angles of the films were measured on a Dataphysics OCA20 contact-angle system at room temperature. Scanning electron

DOI: 10.1021/acsami.5b00155
ACS Appl. Mater. Interfaces 2015, 7, 10718−10726

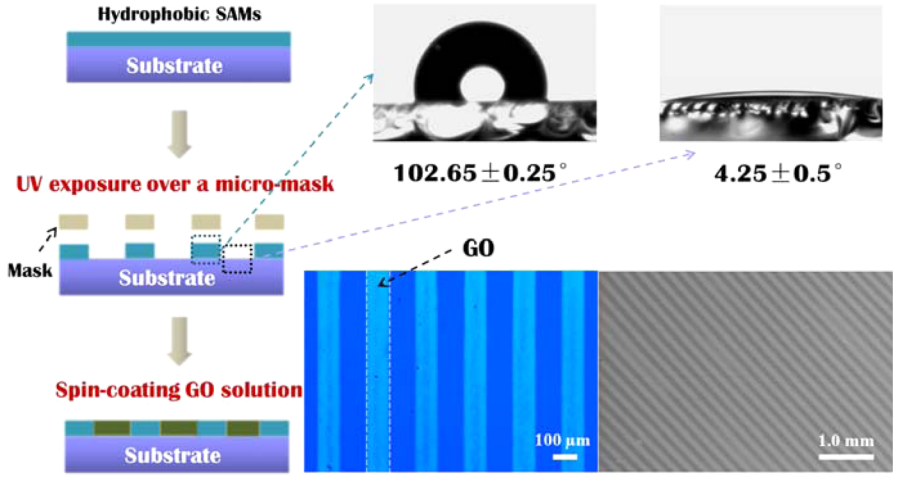

Figure 2. Schematic representation of the GO stripes fabrication, relevant surface properties and stripe pictures.

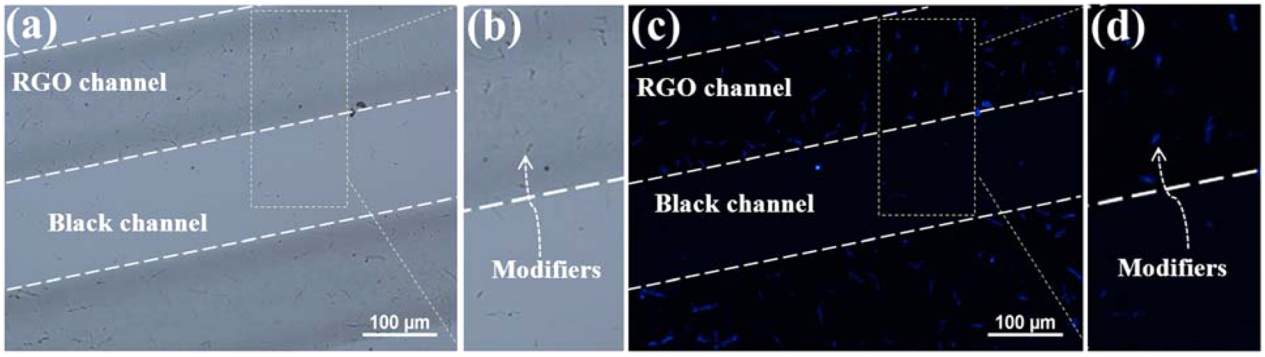

Figure 3. (a) Optical image of the py-diIM-py modified FET. (b) Partial amplification image of the picture shown in panel a (black spots represent modifiers). (c) Fluorescent image of the same device. (d) Partial amplification image shown in panel c (blue spots represent modifiers).

microscopy (SEM) images were taken on a Quanta 200 scanning electron microscopy spectrometer (Philips-FEI). The accelerating voltage was 20 kV, and the emission current was 10 mA. ^{1}H NMR data were obtained by using an AVANCE 400 MHz spectrometer (Bruker). Chemical shifts were referenced to an internal standard, tetramethylsilane (TMS). The MS data were acquired in ESI positive mode and MADI-TOF mode using a Bruker maxis UHR-TOF mass spectrometer. The optical and fluorescence microscopic observations were carried out on a Nikon ECLIPSE Ti−U (Nikon, Japan) with 330−380 nm or 450−490 nm as excitation light.

RESULTS AND DISCUSSION

The fabrication process of solution-gated FET with continuous RGO stripes as micropatterned conductive channels is schematically shown in Figure 1. To generate the micropatterned RGO thin film channels, hydrophilic GO sheets were assembled on a substrate with alternative hydrophilic and hydrophobic microstrips. The patterned substrate was created in the following way: (1) chemical assemble of OTS to prepare hydrophobic self-assembled monolayers (SAMs) on a glass substrate, and (2) treatment of the hydrophobic surface under UV light via a micromask. The SAMs in the unprotected region was decomposed after UV treatment resulting in hydrophilic regions, and the protected region was hydrophobic due to the presence of the SAMs. The surface property of the hydrophilic and hydrophobic regions was confirmed by water contact angle (CA) measurements and the results are shown in Figure 2. The water CAs of the two regions are 4.25 ± 0.5° and 102.65 ± 0.25°, respectively. After the treatment, a GO suspension was selectively adsorbed on the hydrophilic areas. Optical microscopy and SEM studies of micropattern GO stripe film demonstrated that the continuous and uniform GO stripes are successfully achieved, and the stripe structure has a 100 μm width and length up to centimeter scale (c.f. Figure 2). Furthermore, the quality of the GO stripe structure could be controlled and adjusted by varying GO concentration (Figure S1, Supporting Information). Continuous stripes with high quality were acquired when GO concentration was between 0.3 and 1 mg/mL, whereas the stripes with inferior quality were obtained at 0.1 and 0.2 mg/mL.

To obtain conductive RGO strips from the GO strips, reduction reaction was conducted by using hydrazine vapor as a reductant and then annealed in Ar atmosphere. FTIR measurements in transmission mode were utilized to confirm the effective reduction of the GO strips. The results are shown in Figure S2 (Supporting Information). The spectrum of GO illustrates O—H stretching vibration at 3260 cm^{-1} originated from carboxylic acid, and C═O in carboxylic acid and carbonyl moieties at 1736 cm^{-1}. After reduction, the broad O—H stretching band remains, but intensity decreases, and the C═O vibration band even disappears. On the contrary, a new peak at 1570 cm^{-1} appears dramatically close to 1580 cm^{-1}, a characteristic C═C stretching band of graphite, suggesting formation of high quality RGO. This tentative conclusion is further confirmed by the result from XPS measurements (c.f. Figures S3 and S4, Supporting Information). The XPS traces shown in Figure S4a (Supporting Information) reveals that C

DOI: 10.1021/acsami.5b00155
ACS Appl. Mater. Interfaces 2015, 7, 10718−10726

1s signal has three peaks, which could be attributed to carbon atoms of different states: the pristine conjugated C—C (284.8 eV), C in C—O bonds (286.8 eV), and the carbonyl C═O group (288.2 eV), a direct evidence for the obtained GO. However, the intensities of the carbon signal containing oxygen greatly decreased after reduction (Figure S4b, Supporting Information), revealing deoxygenation and restoration of sp^2-hybridized carbons.

Recently, Xu et al. reported a GSFET for detecting ATP, and the detectable concentration range is between 0.002 and 5 mM.[27] The sensitivity of the sensor is not as well as that expected even though it has a number of advantages. For GTP and other NTPs, electronic sensors based on similar devices have not been reported until now. To improve the performance of the GSFET-based NTPs sensors, we introduced a modifier, bis-pyrenyl derivative (py-diIM-py). As shown in Scheme S2 (Supporting Information), the unique structure was based on two pyrenyl units and two cationic imidazole residues of the modifier. It is believed that introduction of the pyrenyl units could enhance attachment of the modifier onto RGO surface due to $\pi-\pi$ interaction, and the cationic structure of the imidazole residues could act as NTPs receptor through electrostatic association. Fluorescence microscopy studies confirmed that the modifier selectively attached on the RGO strips (c.f. Figure 3).

The specific current−voltage ($I-V$) relationships of the RGO and the modified RGO-based devices were tested. The results are shown in Figure S5 (Supporting Information). It is found that both the RGO and the modified RGO devices exhibit electrically continuous Ohmic behaviors. Although modification of the RGO-strips with py-diIM-py increased the resistance of the device, highly stable Ohmic contact is remained, a basis for further studies. To develop the RGO-based FET into usable sensors, FET configuration with solution as top gate was adopted. This is because this configuration is more sensitive than typical back-gate FET.[13] In order to obtain efficient GFET, the stacked layer number of graphene sheet is dominant because it greatly influences the field effect response.[35−37] For the proposed system, the device shows no field effect property when the thickness of the RGO strips exceeds 10 layers of the RGO sheets at 1 mg/mL or even higher concentrations of RGO suspensions. On the other hand, the device prepared in RGO suspensions with concentrations lower than 0.2 mg/mL also show weak or even no field effect response due to inferior continuity of the strips. Optimization tests revealed that 0.3−0.5 mg/mL are suitable concentrations for making a RGO-based FET with superior performances. Figure S6 (Supporting Information) shows typical AFM images and height profiles of the RGO stripe edges. The images and the height profiles indicate that the thickness of the stripe edge prepared at 0.3 mg/mL GO suspension is about 4.6 nm and that prepared at 0.5 mg/mL is about ∼7.7 nm, which correspond to 4−5 layers and 6−7 layers of RGO sheets, respectively (thickness of monolayer GO is ∼1.2 nm in our study, shown in Figure S7, Supporting Information). Considering the electrical property influence of the modifier to the RGO-based FET, the devices prepared in 0.5 mg/mL of GO suspension were chosen for further studies.

The electrical transfer properties of the RGO-based solution-gated FET before and after modification with py-diIM-py were tested, and the results are shown in Figure 4. V-shaped ambipolar field effect behavior from p-type region to n-type region is observed on the RGO-based solution-gated FET, of

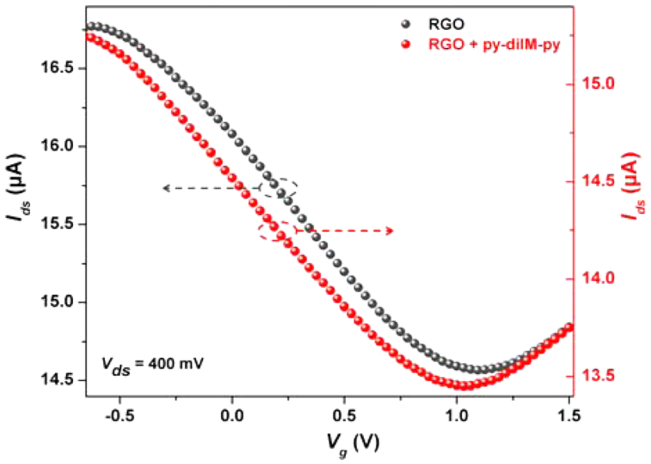

Figure 4. Transfer curves of the RGO-based FET and the py-diIM-py modified RGO-based FET recorded at V_{ds} = 400 mV.

which the characteristic Dirac point appears at ∼1.1 V and the on/off ratio is close to 1.5. These characteristics are similar to GFET, but the Dirac point is right-shift if compared with the value of ideal graphene-based device, showing significant p-type doping. This result could originate from the adsorption of oxygen or water on the RGO surface.[1,38−40] The transfer curves and output curves of the RGO-based solution-gated FET in both p-type and n-type operation are shown in Figure S8 (Supporting Information).

Modification of the RGO-based solution-gated FET with py-diIM-py does not affect its fundamental ambipolar field effect behavior (c.f. Figure 4). However, the conductance (current) of the device decreases and the Dirac point is left-shift, suggesting induction of electrons onto RGO surface due to the existence of interaction between the RGO surface and the modifier, py-diIM-py.

It is already mentioned that RGO is ambipolar material. This characteristic makes it possible to use the RGO-based device in two different ways.[1,19,41] Figure 5a depicts the monitoring results of the modified RGO-based device at different GTP concentrations at either p-type region (V_g = −0.6 V, less than the Dirac voltage) or n-type region (V_g = 1.2 V, greater than the Dirac voltage). It is seen that the current decreased with the addition of GTP when the device operated at p-type region. However, the current increased when it was operated at n-type region. Moreover, the response of the device to the addition of GTP is instantaneous even though equilibrium needs about 5 min. Furthermore, the detection limit to GTP could be as low as 400 nM, which is the lowest value for GTP detection by electronic sensors reported in literature. Figure 5b shows the statistics of the sensor to different concentrations of the analyte, from 4 independent tests at the two different working modes (p-type region and the n-type region). It is seen that the current gradually changes in a wide concentration range (nanomolar scale to micromolar scale), and it tends to be constant when GTP concentration exceeds ca. 50 μM. The probable reason is the adsorption saturation of the analyte on the sensor surface. Besides, the performance of the sensor at p-type region is superior than that at n-type region due to adsorption of oxygen.[20,42] This result is in consistent with that reported by He.[19]

As a control, the sensing performance of the unmodified RGO-based FET to GTP at p-type region was also evaluated. The result is shown in Figure S9 (Supporting Information). It

DOI: 10.1021/acsami.5b00155
ACS Appl. Mater. Interfaces 2015, 7, 10718−10726

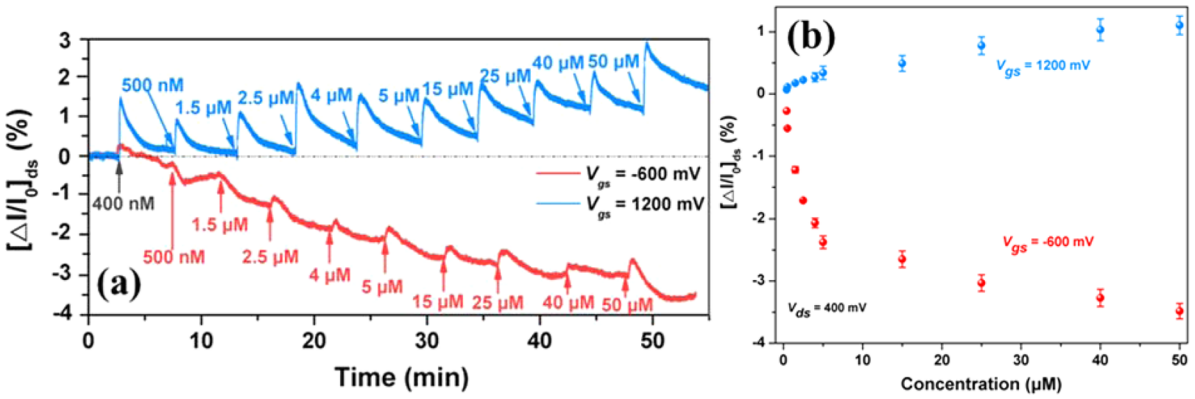

Figure 5. (a) Real-time detection of GTP at various concentrations by the py-diIM-py modified RGO-based FET (V_{ds} = 400 mV, V_g = −600 mV and 1200 mV) and (b) the change of I_{ds} upon the addition of GTP.

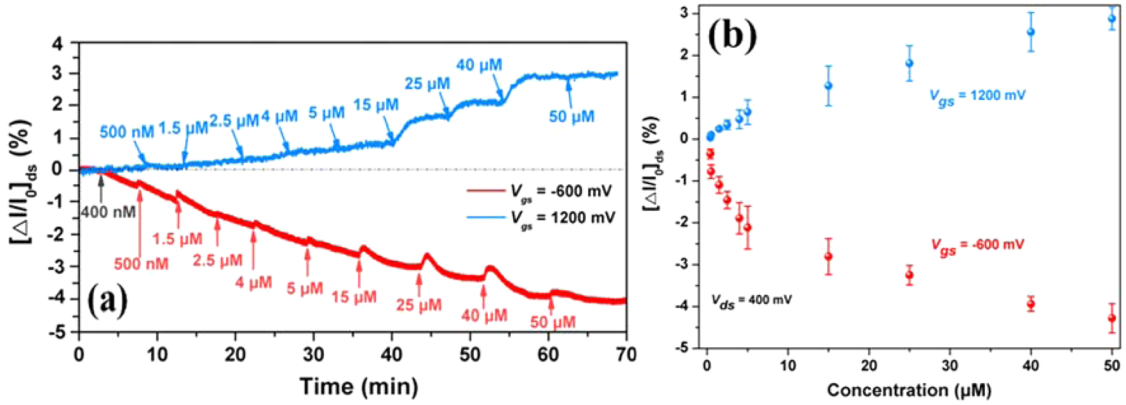

Figure 6. (a) Real-time detection of ATP at various concentrations on the py-diIM-py modified RGO-based FET (V_{ds} = 400 mV, V_g = −600 mV and 1200 mV) and (b) the change of I_{ds} upon the addition of ATP.

can be seen that a similar result was obtained. But the changes in the current are much smaller compared to the result for the modified RGO-based FET. The detection limit for this sensor is ca. 2.5 μM, significantly larger than that for the modified sensor (ca. 400 nM), suggesting efficient enhancement of the modifier, py-diIM-py, to the sensing performance of the FET.

The sensing performance of the modified RGO-based FET sensor for ATP, another important universal energy currency in all of the biological systems, was also examined. As depicted in Figure 6, the real-time response of the modified sensor to the presence of ATP was recorded. The current decreased at *p*-type operation and increased at *n*-type operation, a result similar to the modified device in the exploration of the sensor performance for GTP. Additionally, the detection limit to ATP is 400 nM, and the sensing performance of this sensor to ATP at *p*-type region is also superior to that at *n*-type region. Moreover, similar to that observed in GTP sensing, control experiment for ATP sensing also confirms that py-diIM-py modification benefits the sensing of the RGO-based FET by increasing at least 50% of its sensitivity (c.f. Figure S10, Supporting Information).

The results from the sensing performance studies described above reveal that (1) change in gate voltage of the RGO-based FET not only induces different sensor signals but also modulates the sensor performance, and (2) modification of the RGO-based FET with py-diIM-py is crucial for improving its sensing performance to GTP and ATP.

As already described, the response mode of the RGO-based FET to GTP is similar to ATP no matter if it was operated at a *p*-type region or at an *n*-type region. This is because the two NTPs possess similar chemical structures. For the sensing mechanism, it should not be the electrostatic gating effect as reported in literatures.[19,22,43,44] If the sensing mechanism is based on the electrostatic gate, the increasing current at *p*-type or the decreasing current at *n*-type and the positive shift of Dirac point would be expected since the GTP or ATP with a negatively charged triphosphate group. In fact, opposite results were observed, as already discussed, indicating that a different mechanism was adopted by the studied systems. Specifically, the sensing reason is not the negatively charged triphosphates but the nucleoside in GTP or ATP induces the *n*-doping (or increase of electron concentration) on the RGO. This is consistent with the results in the ATP sensing studies of a GSFET sensor, where graphene was prepared by CVD process.[22] Therefore, the response of the RGO-based FET to the NTPs could be attributed to the stacking interaction between the nucleoside of the analytes and RGO sheets, giving rise to electron transfer from the electron-rich, aromatic bases in GTP or ATP to RGO.

The superior sensing performance of the modified sensor is attributed to the introduction of py-diIM-py enhancing the interaction between the two NTPs and RGO due to electrostatic association of the positively charged modifier and the negatively charged NTPs. In other words, this binding interaction significantly increases the local concentration of ATP or GTP on RGO, which then enhances the electron transfer from the nucleoside to RGO and results in greater current change. The binding interaction of ATP to py-diIM-py

DOI: 10.1021/acsami.5b00155
ACS Appl. Mater. Interfaces 2015, 7, 10718−10726

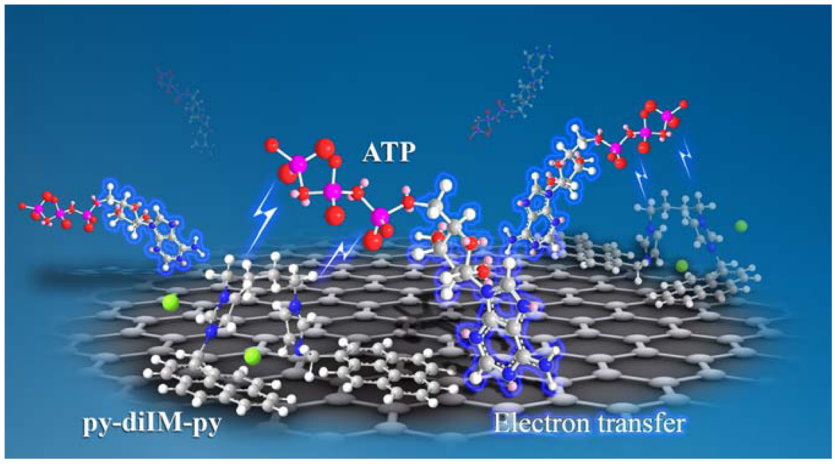

Figure 7. Plausible sensing mechanism of the py-diIM-py modified RGO-based FET to ATP. The electrostatic interaction of ATP with py-diIM-py absorbed on the RGO surface gives rise to effective electron transfer from ATP to RGO.

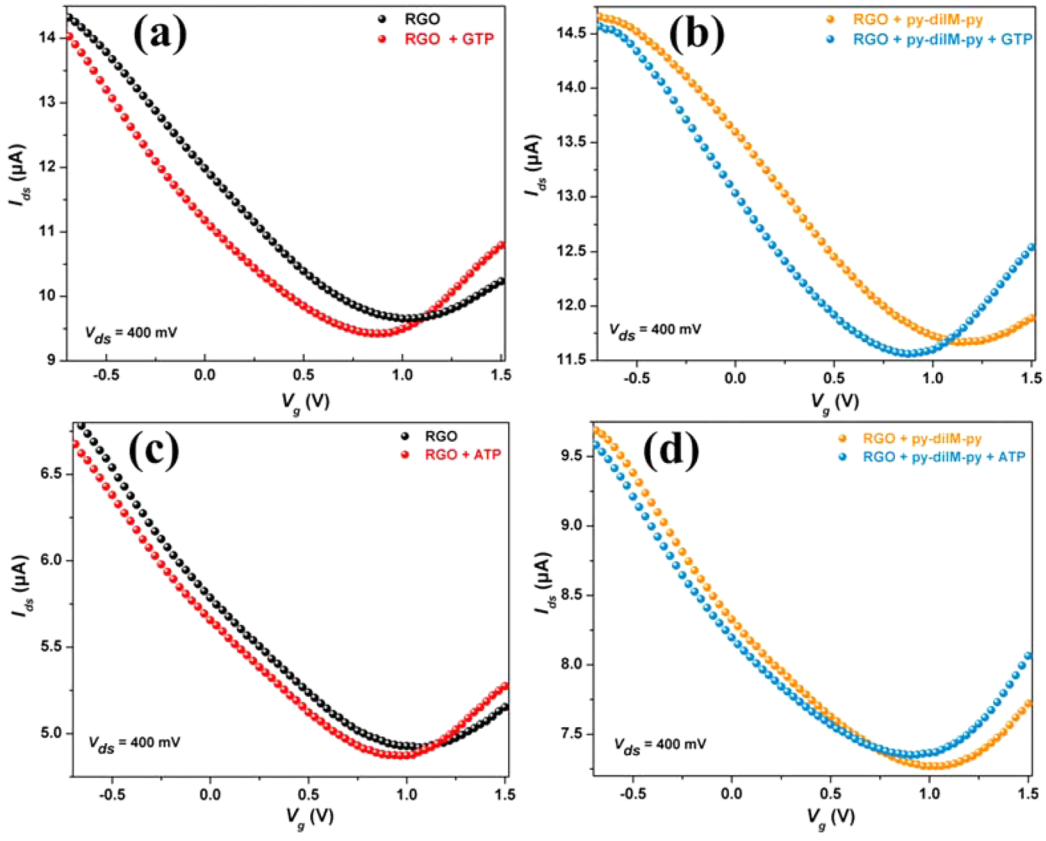

Figure 8. Transfer curves of (a and c) the unmodified RGO-based device and (b and d) the modified RGO-based device before and after addition of GTP or ATP, respectively. The concentration of tested GTP or ATP solution is 50 μM.

is confirmed by changes in zeta potential (Figure S11, Supporting Information). It can be seen that the zeta potential obtained for py-diIM-py is nearly 50 mV (ζ, +49.6 mV), but the introduction of ATP results in 20 mV decrease in the potential (ζ, +29.6 mV), suggesting significant association between the two species. Based on these discussions, a plausible sensing mechanism is proposed and presented in Figure 7.

The fact that the sensing performance of the RGO-based FET to the presence of GTP or ATP is enhanced by the introduction of the modifier py-diIM-py is further supported by a more pronounced change in the transfer curves, as shown in Figure 8. It is seen that although the Dirac points of the two devices all show a left-shift with the addition of GTP or ATP, the modified one causes a more pronounced shift if compared to that of the unmodified one, which illustrates that the modified device is much more sensitive. The data shown in Table 1 is a collection of the values of the Dirac points of the two sensors in the presence of GTP and ATP, respectively.

The responses of the modified and unmodified RGO-based FETs to the presence of different concentrations of five NTPs were examined at *p*-type region (V_{ds} = 0.4 V, V_g = −0.6 V), and the results are shown in Figure 9. It is seen that the responses of the sensors to the NTPs rely on both their concentrations and their chemical nature. In other words, for each NTP, there

DOI: 10.1021/acsami.5b00155
ACS Appl. Mater. Interfaces 2015, 7, 10718−10726

Table 1. Dirac Point Shifts of the Un-modified RGO-based Device and the py-diIM-py Modified RGO-based Device after Addition of GTP and ATP

Dirac point shift	$\delta_{(\text{RGO device})}$ (mV)	$\delta_{(\text{Modified RGO device})}$ (mV)
GTP	−125	−250
ATP	−130	−217

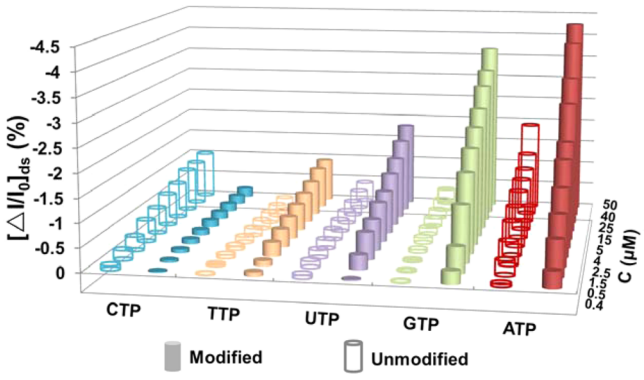

Figure 9. Sensing performances of the unmodified RGO-based and the modified RGO-based devices to NTPs at different concentrations.

is a specific response pattern. Therefore, combining use of the obtained information may result in full discrimination of the NTPs. The variations in the response extent, $(\delta_{\text{modified}} - \delta_{\text{unmodified}})/\delta_{\text{modified}}$, of the two sensors to different NTPs at different concentrations were collectively shown in Figure 10,

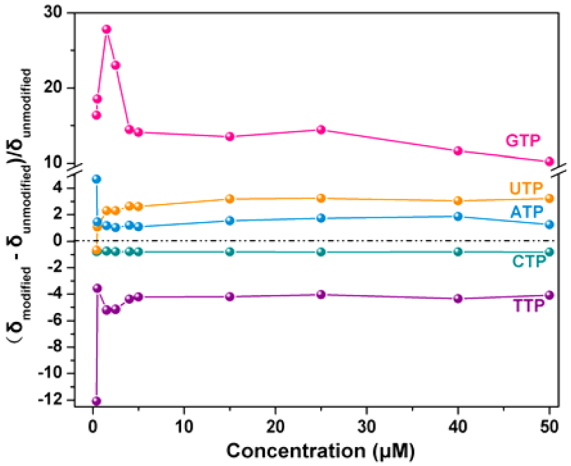

Figure 10. Plots of the variations in response extent before and after py-diIM-py modification of the RGO-based device to different NTPs at various concentrations.

where δ_{modified} and $\delta_{\text{unmodified}}$ are the current variations at a certain concentration of a given NTP on the modified and the unmodified RGO-based devices, respectively. Clearly, detection of GTP is most benefited from the modification of the RGO-based FET as more than 10 times increase in the detection sensitivity. Furthermore, five NTPs over the measured concentration range (1.5−50 μM) are grouped in well-separated lines, illustrating the strong capability of the proposed sensors to discriminate NTPs. This may be the first report on the real-time electronic recognition and discrimination of NTPs based on graphene solution-gated FETs. Actually, for the discrimination of NTPs or nucleotide bases, only two results relevant to graphene-based electronic device were reported, of which one uses graphene nanopore to detect and distinguish nucleic acids or DNA nucleobases,[45,46] and the other utilizes an armchair graphene nanoribbon (AGNR)-based two-dimensional molecular electronics spectroscopy (2D MES) to identify nucleotide bases via variation of bias and/or gate voltages applied to the graphene.[47] Fabrication of the devices as reported in the literatures, however, is complicated and time-consuming when compared with the presented work.

There should be no doubt that the efficient accumulation of NTPs on RGO or py-diIM-py modified RGO surfaces is a prerequirement for the response of the sensors to their presence. The differences in the sensing ability of the two sensors to the five NTPs should be mainly originated from their different binding abilities to the nucleotides. Experimental studies conducted by Sowerby and co-workers demonstrated that graphene possesses a stronger binding ability to G in GTP and A in ATP than those to the nucleosides in other NTPs.[48] The reason for the binding interaction arises from the $\pi-\pi$ stacking between the nucleosides and the RGO, and the conclusion is further confirmed by theoretical calculations performed by Gowtham.[49,50] These conclusions illustrate that the electron transfer from G (A) to RGO could be induced if GTP or ATP adsorbed on RGO effectively. That is why our sensors possess higher sensing sensitivity to the two NTPs. As for the differences in the enhancement of the sensing ability of the sensors to different NTPs after the introduction of py-diIM-py, the reasons might be more complicated. This is because that the presence of the pyrenyl derivative not only alters the binding ability of the graphene surface to the NTPs, but also the orientation of the nucleotide adsorbed. Both the amount of the nucleotide adsorbed and the change of the orientation affect the electron transfer efficiency, which is the origin of the signal change.

CONCLUSION

Two solution-gated FETs with continuous RGO stripes as micropatterned conductive channels were fabricated. The devices could be used as efficient NTPs sensors. The sensing studies showed that modification of the device with py-diIM-py, a positively charged bis-pyrenyl derivative, resulted in significant enhancement in the sensing performance. The modified FET demonstrated a 10-fold enhancement in the sensitivity to GTP and 2-fold increase to ATP. In addition, the detection limit of the two analytes is 400 nM, which is the lowest value for graphene-based electronic sensors reported so far. Moreover, the two devices showed cross-reactive responses to the five NTPs, GTP, ATP, CTP, UTP, and TTP. On the basis of these findings, discrimination of the five NTPs was realized via combining the responses of the two devices. The excellence in sensing performance, simplicity in fabrication and integration in size of the RGO-based solution-gated FET sensors endow the as-prepared devices with great potential in practical detecting NTPs.

ASSOCIATED CONTENT

Supporting Information

Synthesis and characterization of GO and the modifier, py-diIM-py. SEM and AFM images of micropatterned GO stripes, zeta potential data, FT-IR and XPS spectra before and after reduction. The electric properties and sensing performances to GTP or ATP based on the unmodified and modified sensor.

DOI: 10.1021/acsami.5b00155
ACS Appl. Mater. Interfaces 2015, 7, 10718−10726

The Supporting Information is available free of charge on the ACS Publications website at DOI: 10.1021/acsami.5b00155.

AUTHOR INFORMATION

Corresponding Author

*E-mail: yfang@snnu.edu.cn.

Notes

The authors declare no competing financial interest.

ACKNOWLEDGMENTS

We thank the Natural Science Foundation of China (21206089 and 21273141) and the Program for Changjiang Scholars and Innovative Research Team in University (IRT1070). This work was also supported by the Fundamental Research Funds for the Central Universities (GK201301006) and Research Funds of Shaanxi Normal University (X2012YB02).

REFERENCES

(1) Novoselov, K. S.; Geim, A. K.; Morozov, S. V.; Jiang, D.; Zhang, Y.; Dubonos, S. V.; Grigorieva, I. V.; Firsov, A. A. Electric Field Effect in Atomically Thin Carbon Films. *Science* **2004**, *306*, 666−669.

(2) Geim, A. K.; Novoselov, K. S. The Rise of Graphene. *Nat. Mater.* **2007**, *6*, 183−191.

(3) Craciun, M. F.; Russo, S.; Yamamoto, M.; Tarucha, S. Tuneable Electronic Properties in Graphene. *Nano Today* **2011**, *6*, 42−60.

(4) Lee, C.; Wei, X.; Kysar, J. W.; Hone, J. Measurement of the Elastic Properties and Intrinsic Strength of Monolayer Graphene. *Science* **2008**, *321*, 385−388.

(5) Garaj, S.; Hubbard, W.; Reina, A.; Kong, J.; Branton, D.; Golovchenko, J. A. Graphene as a Subnanometre Trans-Electrode Membrane. *Nature* **2010**, *467*, 190−193.

(6) Huang, X.; Zeng, Z.; Fan, Z.; Liu, J.; Zhang, H. Graphene-Based Electrodes. *Adv. Mater.* **2012**, *24*, 5979−6004.

(7) Lee, Y. Y.; Tu, K. H.; Yu, C. C.; Li, S. S.; Hwang, J. Y.; Lin, C. C.; Chen, K. H.; Chen, L. C.; Chen, H. L.; Chen, C. W. Top Laminated Graphene Electrode in a Semitransparent Polymer Solar Cell by Simultaneous Thermal Annealing Releasing Method. *ACS Nano* **2011**, *5*, 6564−6570.

(8) Shanmugam, M.; Jacobs-Gedrim, R.; Song, E. S.; Yu, B. Two-Dimensional Layered Semiconductor/Graphene Heterostructures for Solar Photovoltaic Applications. *Nanoscale* **2014**, *6*, 12682−12689.

(9) Dan, Y.; Lu, Y.; Kybert, N. J.; Luo, Z.; Johnson, A. T. C. Intrinsic Response of Graphene Vapor Sensors. *Nano Lett.* **2009**, *9*, 1472−1475.

(10) Polat, E. O.; Kocabas, C. Broadband Optical Modulators Based on Graphene Supercapacitors. *Nano Lett.* **2013**, *13*, 5851−5857.

(11) Sun, Y.; Wu, Q.; Shi, G. Graphene Based New Energy Materials. *Energy Environ. Sci.* **2011**, *4*, 1113−1132.

(12) Liu, Y. X.; Dong, X. C.; Chen, P. Biological and Chemical Sensors Based on Graphene Materials. *Chem. Soc. Rev.* **2012**, *41*, 2283−2307.

(13) He, Q. Y.; Wu, S. X.; Yin, Z. Y.; Zhang, H. Graphene-Based Electronic Sensors. *Chem. Sci.* **2012**, *3*, 1764−1772.

(14) Eda, G.; Fanchini, G.; Chhowalla, M. Large-Area Ultrathin Films of Reduced Graphene Oxide as a Transparent and Flexible Electronic Material. *Nat. Nanotechnol.* **2008**, *3*, 270−274.

(15) Schedin, F.; Geim, A. K.; Morozov, S. V.; Hill, E. W.; Blake, P.; Katsnelson, M. I.; Novoselov, K. S. Detection of Individual Gas Molecules Adsorbed on Graphene. *Nat. Mater.* **2007**, *6*, 652−655.

(16) Yu, C. M.; Guo, Y. L.; Liu, H. T.; Yan, N.; Xu, Z. Y.; Yu, G.; Fang, Y.; Liu, Y. Q. Ultrasensitive and Selective Sensing of Heavy Metal Ions with Modified Graphene. *Chem. Commun.* **2013**, *49*, 6492−6494.

(17) Zhou, G. H.; Chang, J. B.; Cui, S. M.; Pu, H. H.; Wen, Z. H.; Chen, J. H. Real-Time, Selective Detection of Pb^{2+} in Water Using a Reduced Graphene Oxide/Gold Nanoparticle Field-Effect Transistor Device. *ACS Appl. Mater. Interfaces* **2014**, *6*, 19235−19241.

(18) Chen, Y. N.; Michael, Z. P.; Kotchey, G. P.; Zhao, Y.; Star, A. Electronic Detection of Bacteria Using Holey Reduced Graphene Oxide. *ACS Appl. Mater. Interfaces* **2014**, *6*, 3805−3810.

(19) He, Q. Y.; Sudibya, H. G.; Yin, Z. Y.; Wu, S. X.; Li, H.; Boey, F.; Huang, W.; Chen, P.; Zhang, H. Centimeter-Long and Large-Scale Micropatterns of Reduced Graphene Oxide Films: Fabrication and Sensing Applications. *ACS Nano* **2010**, *4*, 3201−3208.

(20) Park, S. J.; Kwon, O. S.; Lee, S. H.; Song, H. S.; Park, T. H.; Jang, J. Ultrasensitive Flexible Graphene Based Field-Effect Transistor (FET)-Type Bioelectronic Nose. *Nano Lett.* **2012**, *12*, 5082−5090.

(21) Jiang, H. J. Chemical Preparation of Graphene-Based Nanomaterials and Their Applications in Chemical and Biological Sensors. *Small* **2011**, *7*, 2413−2427.

(22) Dong, X. C.; Shi, Y. M.; Huang, W.; Chen, P.; Li, L. J. Electrical Detection of DNA Hybridization with Single-Base Specificity Using Transistors Based on CVD-Grown Graphene Sheets. *Adv. Mater.* **2010**, *22*, 1649−1653.

(23) Yin, Z. Y.; He, Q. Y.; Huang, X.; Zhang, J.; Wu, S. X.; Chen, P.; Lu, G.; Chen, P.; Zhang, Q. C.; Yan, Q. Y.; Zhang, H. Real-Time DNA Detection Using Pt Nanoparticle-Decorated Reduced Graphene Oxide Field-Effect Transistors. *Nanoscale* **2012**, *4*, 293−297.

(24) Huang, Y. X.; Dong, X. C.; Shi, Y. M.; Li, C. M.; Li, L. J.; Chen, P. Nanoelectronic Biosensors Based on CVD Grown Graphene. *Nanoscale* **2010**, *2*, 1485−1488.

(25) Ohno, Y.; Maehashi, K.; Yamashiro, Y.; Matsumoto, K. Electrolyte-Gated Graphene Field-Effect Transistors for Detecting pH and Protein Adsorption. *Nano Lett.* **2009**, *9*, 3318−3322.

(26) Ohno, Y.; Maehashi, K.; Matsumoto, K. Label-Free Biosensors Based on Aptamer-Modified Graphene Field-Effect Transistors. *J. Am. Chem. Soc.* **2010**, *132*, 18012−18013.

(27) Xu, S. C.; Man, B. Y.; Jiang, S. Z.; Yue, W. W.; Yang, C.; Liu, M.; Chen, C. S.; Zhang, C. Direct Growth of Graphene on Quartz Substrates for Label-Free Detection of Adenosine Triphosphate. *Nanotechnology* **2014**, *25* (10), 165702.

(28) Kim, S. K.; Lee, D. H.; Hong, J. I.; Yoon, J. Y. Chemosensors for Pyrophosphate. *Acc. Chem. Res.* **2009**, *42*, 23−31.

(29) Gunnlaugsson, T.; Glynn, M.; Tocci (née Hussey), G. M.; Kruger, P. E.; Pfeffer, F. M. Anion Recognition and Sensing in Organic and Aqueous Media Using Luminescent and Colorimetric Sensors. *Coord. Chem. Rev.* **2006**, *250*, 3094−3117.

(30) Li, C.; Numata, M.; Takeuchi, M.; Shinkai, S. A Sensitive Colorimetric and Fluorescent Probe Based on a Polythiophene Derivative for the Detection of ATP. *Angew. Chem., Int. Ed.* **2005**, *44*, 6371−6374.

(31) Mizukami, S.; Nagano, T.; Urano, Y.; Odani, A.; Kikuchi, K. A Fluorescent Anion Sensor That Works in Neutral Aqueous Solution for Bioanalytical Application. *J. Am. Chem. Soc.* **2002**, *124*, 3920−3925.

(32) Liu, J.; Morikawa, M.; Kimizuka, N. Conversion of Molecular Information by Luminescent Nanointerface Self-Assembled from Amphiphilic Tb(III) Complexes. *J. Am. Chem. Soc.* **2011**, *133*, 17370−17374.

(33) Lei, H. R.; Liu, J.; Yan, J. L.; Lu, S. H.; Fang, Y. Luminescent Vesicular Nanointerface: A Highly Selective and Sensitive "Turn-on" Sensor for Guanosine Triphosphate. *ACS Appl. Mater. Interfaces* **2014**, *6*, 13642−13647.

(34) Banoub, J. H.; Newton, R. P.; Esmans, E.; Ewing, D. F.; Mackenzie, G. Recent Developments in Mass Spectrometry for the Characterization of Nucleosides, Nucleotides, Oligonucleotides, and Nucleic Acids. *Chem. Rev.* **2005**, *105*, 1869−1915.

(35) Eda, G.; Fanchini, G.; Chhowalla, M. Large-Area Ultrathin Films of Reduced Graphene Oxide as a Transparent and Flexible Electronic Material. *Nat. Nanotechnol.* **2008**, *3*, 270−274.

(36) Zhang, J.; Hu, P. A.; Zhang, R. F.; Wang, X. N.; Yang, B.; Cao, W. W.; Li, Y. B.; He, X. D.; Wang, Z. L.; O'Neill, W. Soft-Lithographic Processed Soluble Micropatterns of Reduced Graphene Oxide for Wafer-Scale Thin Film Transistors and Gas Sensors. *J. Mater. Chem.* **2012**, *22*, 714−718.

(37) He, Q. Y.; Wu, S. X.; Gao, S.; Cao, X. H.; Yin, Z. Y.; Li, H.; Chen, P.; Zhang, H. Transparent, Flexible, All-Reduced Graphene Oxide Thin Film Transistors. *ACS Nano* **2011**, *5*, 5038−5044.
(38) Yang, W. R.; Ratinac, K. R.; Ringer, S. P.; Thordarson, P.; Gooding, J. J.; Braet, F. Carbon Nanomaterials in Biosensors: Should You Use Nanotubes or Graphene? *Angew. Chem., Int. Ed.* **2010**, *49*, 2114−2138.
(39) Wei, D. C.; Liu, Y. Q. Controllable Synthesis of Graphene and Its Applications. *Adv. Mater.* **2010**, *22*, 3225−3241.
(40) Ryu, S.; Liu, L.; Berciaud, S.; Yu, Y. J.; Liu, H. T.; Kim, P.; Flynn, G. W.; Brus, L. E. Atmospheric Oxygen Binding and Hole Doping in Deformed Graphene on a SiO_2 Substrate. *Nano Lett.* **2010**, *10*, 4944−4951.
(41) Sudibya, H. G.; He, Q. Y.; Zhang, H.; Chen, P. Electrical Detection of Metal Ions Using Field-Effect Transistors Based on Micropatterned Reduced Graphene Oxide Films. *ACS Nano* **2011**, *5*, 1990−1994.
(42) An, J. H.; Park, S. J.; Kwon, O. S.; Bae, J.; Jang, J. High-Performance Flexible Graphene Aptasensor for Mercury Detection in Mussels. *ACS Nano* **2013**, *7*, 10563−10571.
(43) Artyukhin, A. B.; Stadermann, M.; Friddle, R. W.; Stroeve, P.; Bakajin, O.; Noy, A. Controlled Electrostatic Gating of Carbon Nanotube FETs. *Nano Lett.* **2006**, *6*, 2080−2085.
(44) Heller, I.; Janssens, A. M.; Mannik, J.; Minot, E. D.; Lemay, S. G.; Dekker, C. Identifying the Mechanism of Biosensing with Carbon Nanotube Transistors. *Nano Lett.* **2008**, *8*, 591−595.
(45) Ying, Y. L.; Zhang, J. J.; Gao, R.; Long, Y. T. Nanopore-Based Sequencing and Detection of Nucleic Acids. *Angew. Chem., Int. Ed.* **2013**, *52*, 13154−13161.
(46) Sadeghi, H.; Algaragholy, L.; Pope, T.; Bailey, S.; Visontai, D.; Manrique, D.; Ferrer, J.; Garcia-Suarez, V.; Sangtarash, S.; Lambert, C. J. Graphene Sculpturene Nanopores for DNA Nucleobase Sensing. *J. Phys. Chem. B* **2014**, *118*, 6908−6914.
(47) Rajan, A. C.; Rezapour, M. R.; Yun, J.; Cho, Y.; Cho, W. J.; Min, S. K.; Lee, G.; Kim, K. S. Two Dimensional Molecular Electronics Spectroscopy for Molecular Fingerprinting, DNA Sequencing, and Cancerous DNA Recognition. *ACS Nano* **2014**, *8*, 1827−1833.
(48) Sowerby, S. J.; Cohn, C. A.; Heckl, W. M.; Holm, N. G. Differential Adsorption of Nucleic Acid Bases: Relevance to the Origin of Life. *Proc. Natl. Acad. Sci. U.S.A.* **2001**, *98*, 820−822.
(49) Antony, J.; Grimme, S. Structures and Interaction Energies of Stacked Graphene−Nucleobase Complexes. *Phys. Chem. Chem. Phys.* **2008**, *10*, 2581−2583.
(50) Gowtham, S.; Scheicher, R. H.; Ahuja, R.; Pandey, R.; Karna, S. P. Physisorption of Nucleobases on Ggraphene: Density-Functional Calculations. *Phys. Rev. B* **2007**, *76* (3), 033401.

DOI: 10.1021/acsami.5b00155
ACS Appl. Mater. Interfaces 2015, 7, 10718−10726